GSA Data Repository 2018186

Gas hydrates in coarse-grained reservoirs interpreted from velocity pull up: Mississippi Fan, Gulf of Mexico

Andrew S. Madof

METHODS

Petrophysical calculations

Well-log interpretation was conducted on the GC 955-H well using commercial petrophysical analysis software (Geolog® by Paradigm®). Porosity was calculated from density via the following equation:

$$\phi = \frac{\rho_{ma} - \rho_b}{\rho_{ma} - \rho_f}$$

where ϕ is porosity, ρ_{ma} is the density of the matrix (2.65 g/cc – sandstone), ρ_b is the bulk density (measured from the density-logging tool), and ρ_f is the density of the fluid (1.00 g/cc – water). Archie's equation was subsequently used to solve for gas hydrate saturation via the following relationships:

$$S_w = \sqrt{\frac{a\, R_w}{\phi^m\, R_t}}$$

$$S_{gh} = 1 - S_w$$

where S_w is water saturation, a is the Tortuosity coefficient (equal to 1), R_w is the electrical resistivity of the formation water, ϕ is porosity (calculated from density), m is a cementation exponent (equal to 2), R_t is the electrical resistivity of the formation (measured from

deep resistivity), and S_{gh} is gas hydrate saturation. Results of the calculations are displayed in Fig. DR2.

Seismic interpretation

Reflections were mapped on full-stack zero-phase seismic data (two-way travel time) using commercial seismic-interpretation software (SeisEarth® by Paradigm®). High-amplitude peak reflections were used to trace the top of channelized systems P1-P3, as well as Reflections 1,2 and 4 (R1, R2, and R4). High-amplitude trough reflections were selected to map the base of the P1-P3 systems, as well as Reflection 3 (R3 – see Fig. DR8B).

Root mean squared (RMS) amplitude and spectral decomposition were calculated on the 3D seismic volume (Figs. 2C and DR7A). RMS was calculated on the interval from the base of the gas hydrate stability zone to the sea floor using SeisEarth® by Paradigm®. Spectral decomposition was calculated over the entire dataset and calibrated to the upper unit of the P3 system using commercial seismic-interpretation software (GeoTeric® by Foster Findlay Associates).

Wavelength filtering

To isolate VPU, R1-R4 (Fig. DR8B) were filtered and stacked using commercial geophysical-interpretation software (OasisMontaj® by GeoSoft®). Individual surfaces were filtered via a high-pass Butterworth filter, with a wavelength of 75 km (46.6 mi) and a filter order of 5. The average of the four surfaces is displayed as a single surface in Fig. 2D.

REFRENCES CITED

Dai, J., Xu, H., Snyder, F., and Dutta, N., 2004, Detection and estimation of gas hydrates using rock physics and seismic inversion: Examples from the northern deepwater Gulf of Mexico: The Leading Edge, v. 23, p. 60-66.

Guerin, G., Cook, A., Mrozewski, S., Collett, T., and Boswell, R., 2009, Gulf of Mexico gas hydrate joint industry project leg II: Green Canyon 955 LWD operations and results: https://www.netl.doe.gov/File%20Library/Research/Oil-Gas/methane%20hydrates/GC955LWDOps.pdf (April 2018).

Jones, I.F., 2012, Tutorial: Incorporating near-surface velocity anomalies in pre-stack depth migration models: First Break, v. 30, p. 47-58.

Lee, M.W., Hutchinson, D.R., Collett, T.S., and Dillon, W.P., 1996, Seismic velocities for hydrate-bearing sediments using weighted equation: Journal of Geophysical Research, v., 101, p. 20347-20358.

Kvenvolden, K.A., and McMenamin, M.A., 1980, Hydrates of natural gas: A review of their geological occurrences: United States Geological Survey Circular 825, 11 p.

Madof, A.S., 2016a, Methods and systems for identifying a clathrate deposit, United States Patent application 15/218910, filed July 25, 2016.

Madof, A.S., 2016b, Methods and systems for quantifying a clathrate deposit, United States Patent application 15/218920, filed July 25, 2016.

Shaw, J.H., Connors, C., and Suppe, J., eds., 2005, Seismic interpretation of contractional fault-related folds: An AAPG Seismic Atlas: American Association of Petroleum Geologists Studies in Geology 53, 157 p.

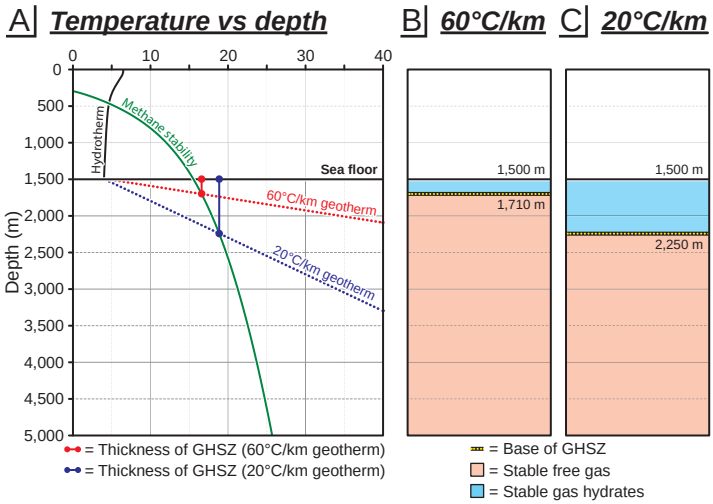

Figure DR1. Gas hydrate stability zone (GHSZ) in the marine setting, modeled with 100% methane (modified from Kvenvolden and McMenamin, 1980). A: Model is constructed using a sea-floor depth of 1,500 m (4°C at the sea floor) and geotherms of 60°C/km (B) and 20°C/km (C). The 60°C/km geotherm (B) yields a 210-m thick GHSZ, compared to the 20°C/km geotherm (i.e., 750-m thick GHSZ). The 20°C/km model (C) is used for the study area, and is displayed in Figs. 1B, 2B, DR8B, and DR10B.

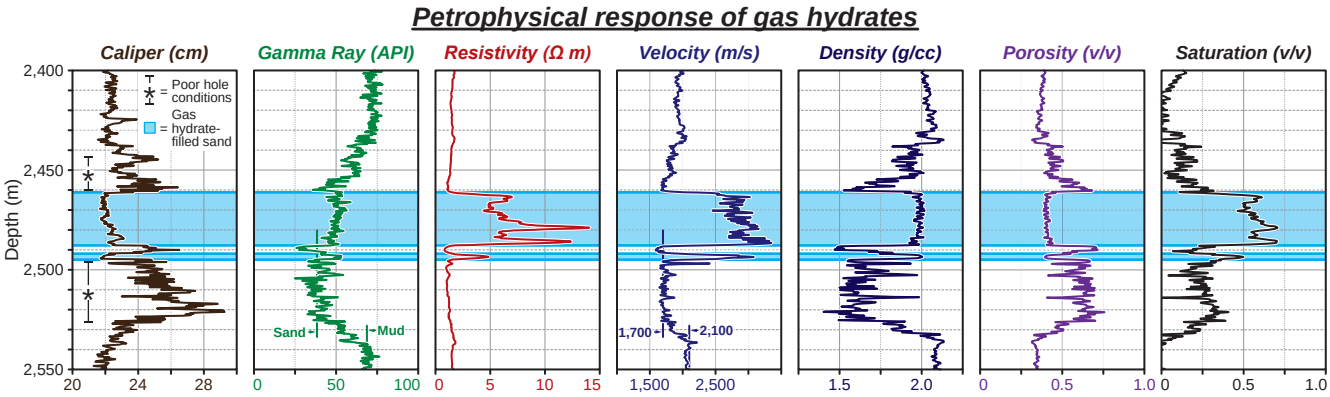

Figure DR2. Petrophysical response of a gas hydrate-bearing sandy reservoir from the GC 955-H well in the northern Gulf of Mexico (modified from Guerin et al., 2009 - see Fig. 1A for location). Gas hydrate-bearing sediments are identified primarily based on elevated values of resistivity (>5 Ω m) and P-wave velocity (>2,500 m/s) that coincide with depressed gamma ray measurements (<50 API). Although poor-hole conditions inevitably lead to erroneous measurements, velocities of non-gas hydrate-bearing sediments (i.e., background) are taken as 1,700 m/s (sand) and 2,100 m/s (mud); these values are used as input for Models 1-4 (see Fig. 3). See Methods section for calculations regarding porosity and saturation.

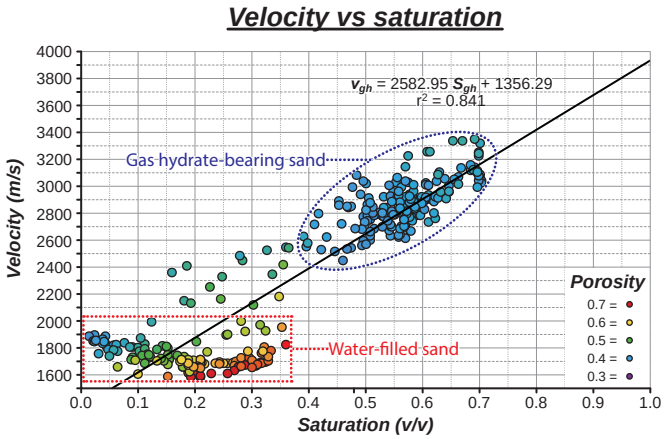

Figure DR3. Crossplot of P-wave velocity (v_{gh}) versus saturation (S_{gh}) for the 2,450-2,500-m depth interval in the GC 955-H well (see Fig. DR2). The data show a linear relationship, with gas hydrate-bearing sand corresponding to values of increased velocity (>2,500 m/s) and decreased porosity (<0.5). The relationship is used to calibrate saturation to velocity in Fig. 3.

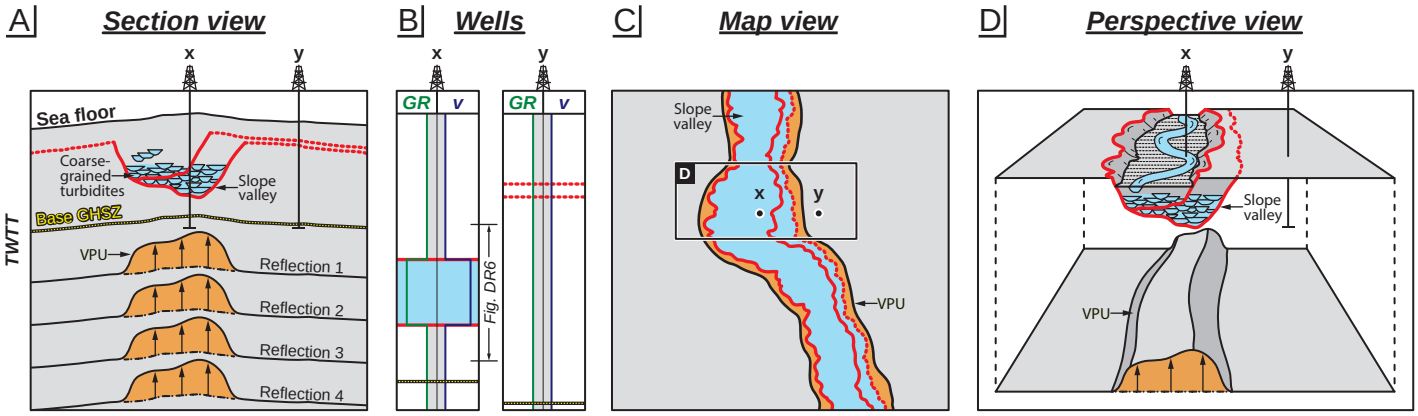

Figure DR4. Diagram illustrating velocity pull up (VPU) in two-way travel time (TWTT - modified from Madof, 2016a and 2016b). A: Gas hydrate-bearing coarse-grained turbidites (blue - high velocity) are encased in background sediments (gray - low velocity) and create travel-time deficits resulting in convex reflections at depth (orange). Major erosional surfaces defining slope valleys are shown as solid red lines; time-equivalent non-erosional components are illustrated as red dashed lines. Solid black lines associated with Reflections 1-4 show surfaces in TWTT; dash-dot lines under VPU show the surfaces in depth (i.e., velocity effect removed). B: Two idealized well logs showing gamma ray (GR) and P-wave velocity (v) trends. Well x encounters gas hydrate-bearing sediments and results in values of decreased gamma ray and increased velocity. Well y is located lateral to gas hydrate-bearing system, and shows no change in petrophysical character. C: Map-view image of two slope valleys and underlying VPU. D: Perspective view of the gas hydrate system; thicker gas hydrate-bearing sediments correspond to higher values of VPU.

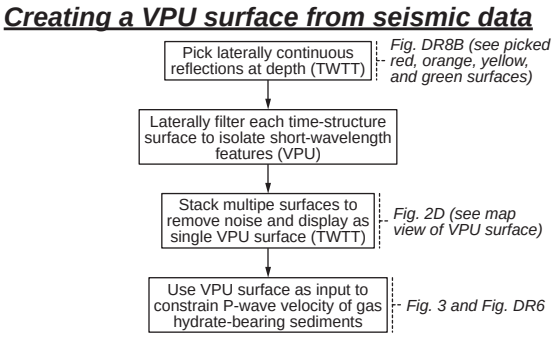

Figure DR5. Flowchart showing steps necessary to create VPU surface from seismic data (TWTT). Short-wavelength features (VPU) on time-structure surfaces are isolated via a high-pass filter using geophysical software (e.g., OasisMontaj by GeoSoft® - see Methods section). Magnitude is measured directly from VPU surface (see Fig. 2D) and used as input to solve for P-wave velocity of gas hydrate-bearing sediments (see Fig. DR6).

Calculating P-wave velocity of gas hydrate-bearing sediments using VPU

Step 1: Estimate Th(t)

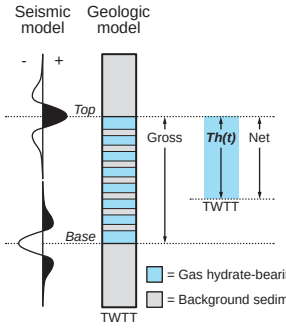

Where:

Th(t) *= Net thickness of gas hydrate-bearing sediments (TWTT)**

* = Calculated by multiplying gross thickness (from seismic) by net:gross (from analog)

Step 2: Express v_{gh} in terms of v_b

$$v_{gh} = b\, v_b \quad \text{(Eq. 1)}$$

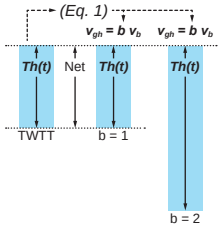

Where:

v_{gh} *= P-wave velocity of gas hydrate-bearing sediments***

b *= Scalar relating velocities of background sediments to gas hydrate-bearing sediments****

v_b *= P-wave velocity of background sediments*****

** = Unknown

*** = Although there exists a complex three-dimensional relationship between v_s and v_p, the one-dimensional model presented here provides a simplification by treating values as linear

**** = Estimated from checkshot, velocity function, or analog

Step 3: Relate Th(t) to VPU(t)

$$VPU(t) = \left(\frac{v_{gh}}{v_b} - 1\right) Th(t) \quad \text{(Eq. 2)}$$

Where:

VPU(t) *= Velocity pull up (TWTT)†*

Substitute Eq. 1 into Eq. 2:

$$VPU(t) = \left(\frac{b\, v_b}{v_b} - 1\right) Th(t) \quad \text{(Eq. 3)}$$

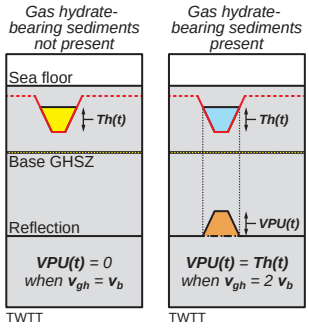

† = To calculate a VPU(t) surface, see Fig. DR5

Step 4: Solve for b

$$b = \frac{VPU(t)}{Th(t)} + 1 \quad \text{(Eq. 4)}$$

Note that in order to solve for v_{gh} *(Eq. 1) based on* b *(Eq. 4), three quantities are needed:*

(i) v_b *- estimated from checkshot, velocity function, or analog*

(ii) ***Th(t)*** *- measured from seismic (TWTT) and multiplied by net:gross*

(iii) ***VPU(t)*** *- calculated from stacked and filtered time-structure surfaces*

Step 5: Correlate VPU(t) to Th(t)††

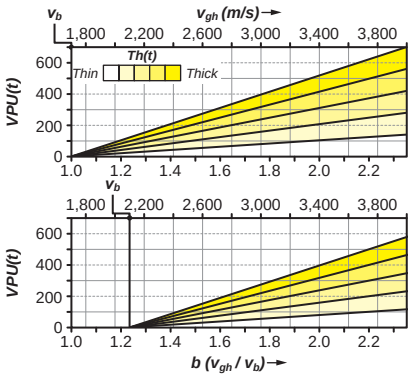

Low-velocity (v_b) model

High-velocity (v_b) model

†† = For detailed graphs, see Fig. DR9

Step 6: Substitute S_{gh} for v_{gh}

To relate v_{gh} *to* S_{gh} *(i.e., saturation of gas hydrate-bearing sediments), use empirical relationships†††, rock-physics models, or theoretical correlations:*

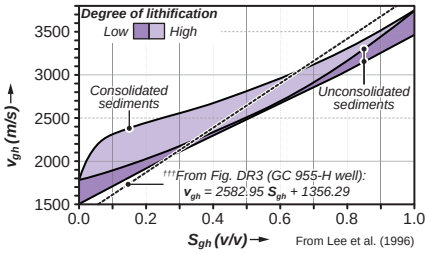

From Lee et al. (1996)

Step 7: Example

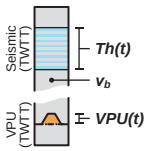

Inputs:	*Solution:*	
v_b *= 1,700 m/s*	b *= 1.5*	*(Eq. 4)*
Th(t) *= 200 ms (TWTT) x 0.50 (net:gross) = 100 ms*	$v_{gh} = b\, v_b$ *= (1.5) (1,700 m/s) = 2,550 m/s*	*(Eq. 1)*
VPU(t) *= 50 ms*	S_{gh} *= 0.46*	*(Eq. from Fig. DR3)*

Figure DR6. Schematic diagram showing derivation of equations used to solve for P-wave velocity of gas hydrate-bearing sediments. Velocity is solved for using VPU(t) and Th(t) (Steps 1-5), and is related to saturation using empirical relationships, rock-physics models, or theoretical correlations (Step 6 - see Lee et al., 1996 and Dai et al., 2004 for details). An example (in the absence of well control) is provided to further illustrate the concept (Step 7).

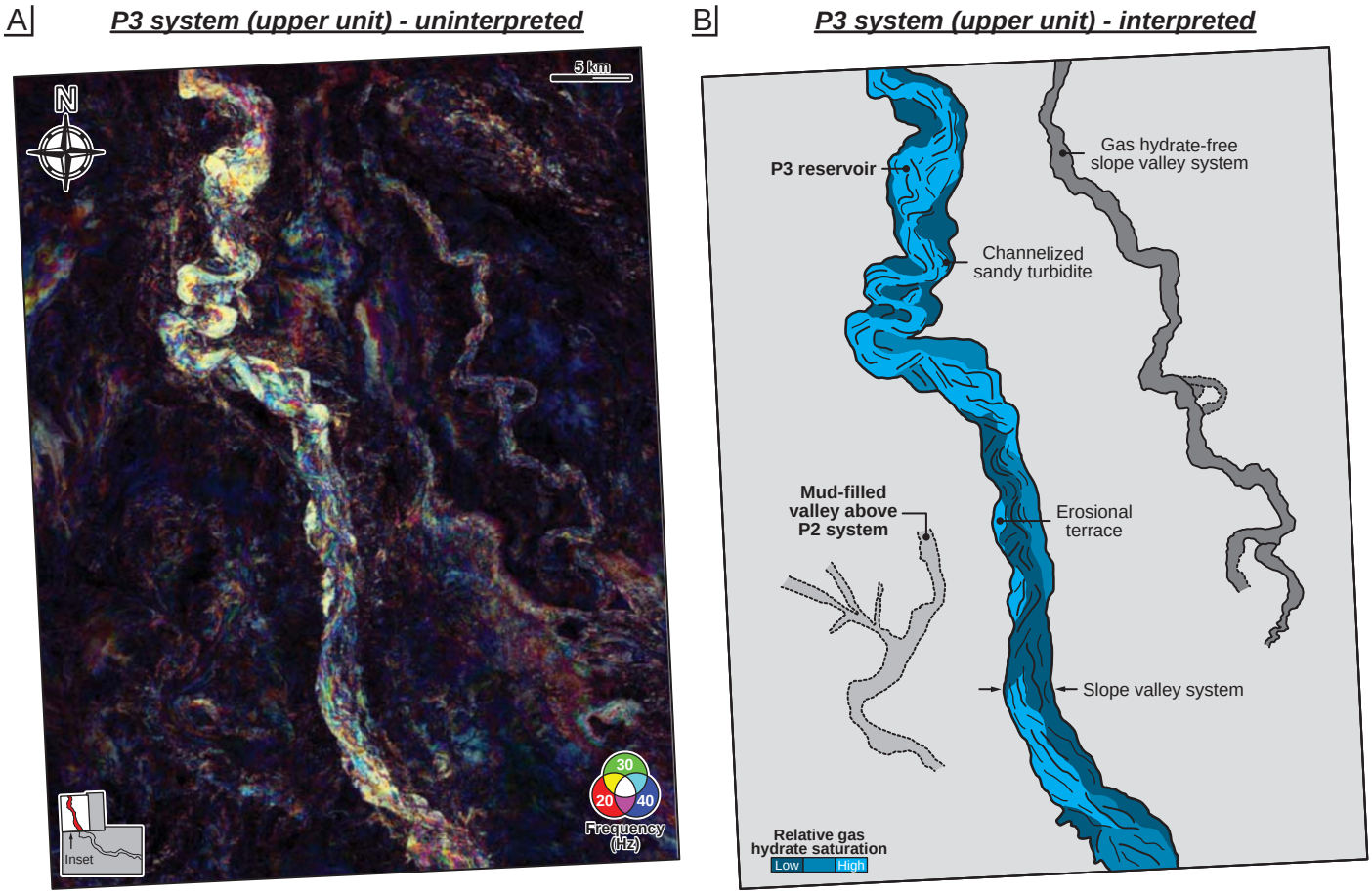

Figure DR7. Map-view image (time slice) of the upper unit of the P3 system. A: Spectral decomposition of zero-phase full-stack seismic data (TWTT) showing sinuous high-amplitude high-frequency reflections. B: Interpretation showing variably saturated gas hydrate accumulations contained within the meandering P3 slope valley system. Deposits with the highest saturation (qualitatively based on amplitude and frequency) are located towards the north, and are situated westward of a gas hydrate-free slope valley system.

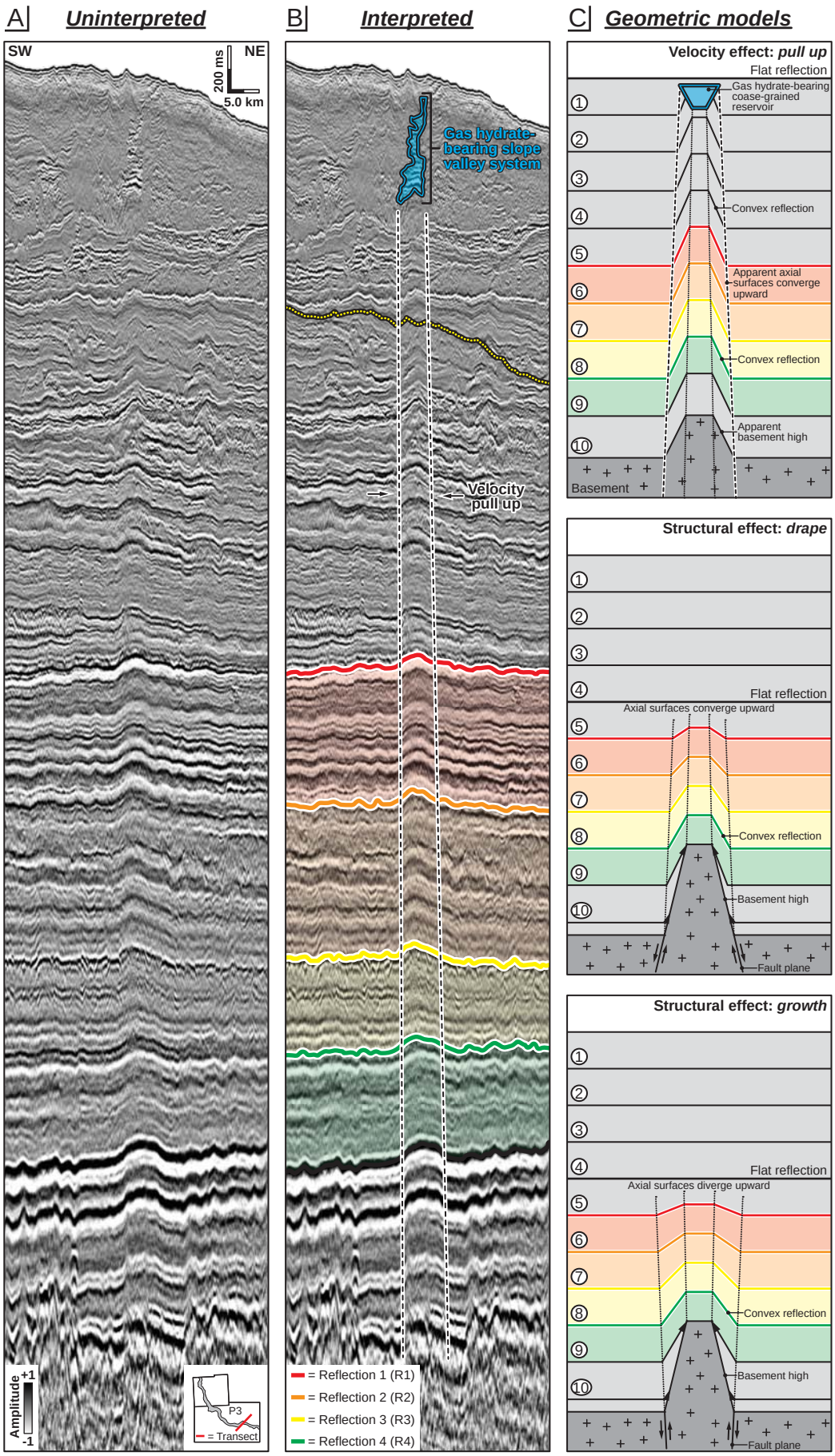

Figure DR8. Seismic section and geometric models of a portion of the central Gulf of Mexico, showing convex reflections at depth. Features are interpreted to be VPU associated with gas hydrate accumulation in the P3 reservoir. A: Uninterpreted zero-phase full-stack seismic section (TWTT). B: The section is interpreted to contain gas hydrate-bearing slope valley systems, resulting in underlying VPU that extends to the basement (i.e., 5,000 ms below the deposit). Because the average widths of P1-P3 systems (see Fig. 2C) are greater than that of the seismic streamer length (i.e., 6,000 m/19,685 ft), acquisition undershoot does not preclude imaging the accumulations. Yellow-black dotted line delineates the base of the GHSZ. C (top): Model showing gas hydrate-bearing coarse-grained reservoir responsible for underlying convex reflections (i.e., VPU). Apparent axial surfaces converge upward, intersect layers 1-10, and extend from the base of the deposit to the basement. The model is consistent with observations from (A), particularly in that convexity increases in magnitude and width with depth; this trend is a diagnostic feature of shallow high-velocity deposits (see Jones, 2012). Models showing reflection geometries associated with a drape onto a basement high (C - middle), and growth away from a basement high (C - bottom) (see Shaw et al., 2006). In these scenarios, axial surfaces associated with deformation are discontinuous above layer 5, and are therefore inconsistent with observations from (A).

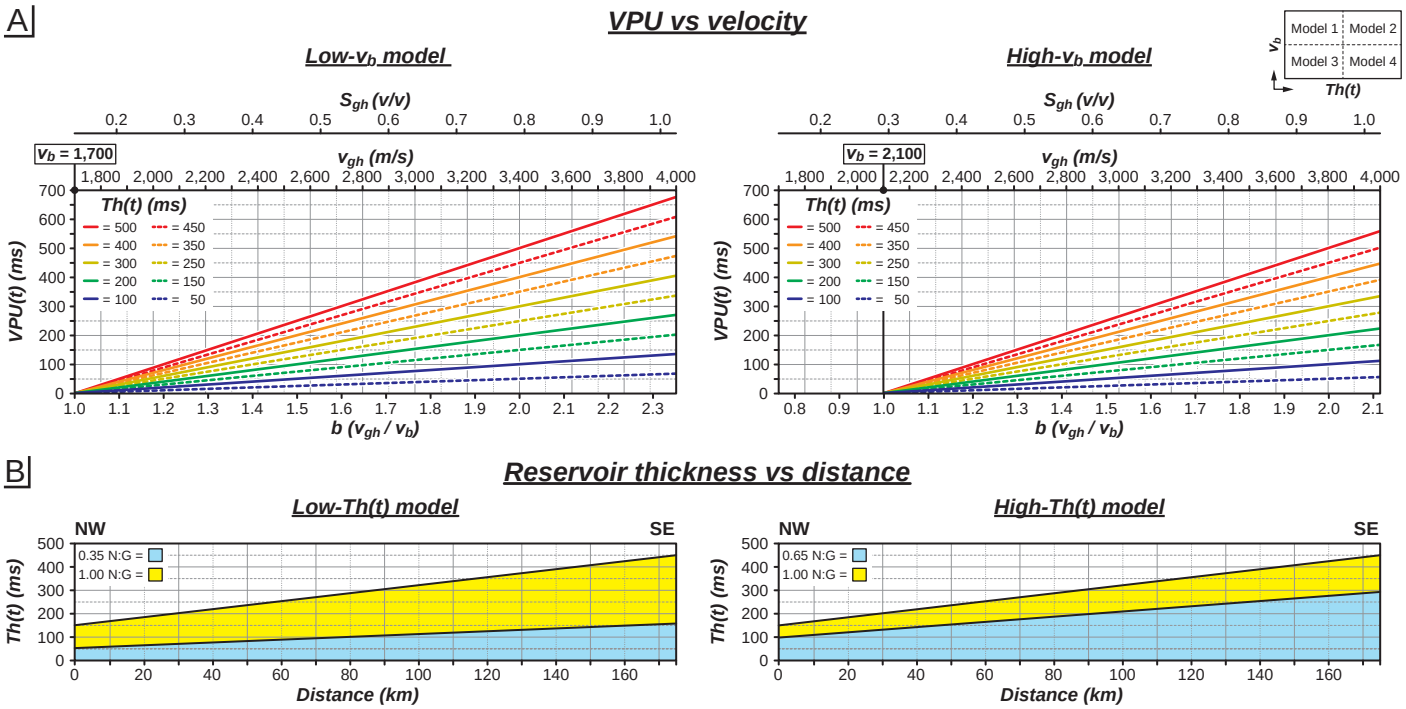

Figure DR9. Inputs for calculating the P-wave velocity of gas hydrate-bearing sediments (see Fig. 3). A: VPU versus velocity of gas hydrate-bearing sediments using a low- and high-velocity background. Colored lines represent iso-values of reservoir thickness and show a linear relationship. Background velocity values are calibrated to the GC 955-H well (Fig. DR2). B: Two models for the P3 reservoir with a net:gross (N:G) thickness of 0.35 (left) and 0.65 (right); the gross thickness of the reservoir ranges from 150 ms (TWTT - NW) to 450 ms (TWTT - SE).

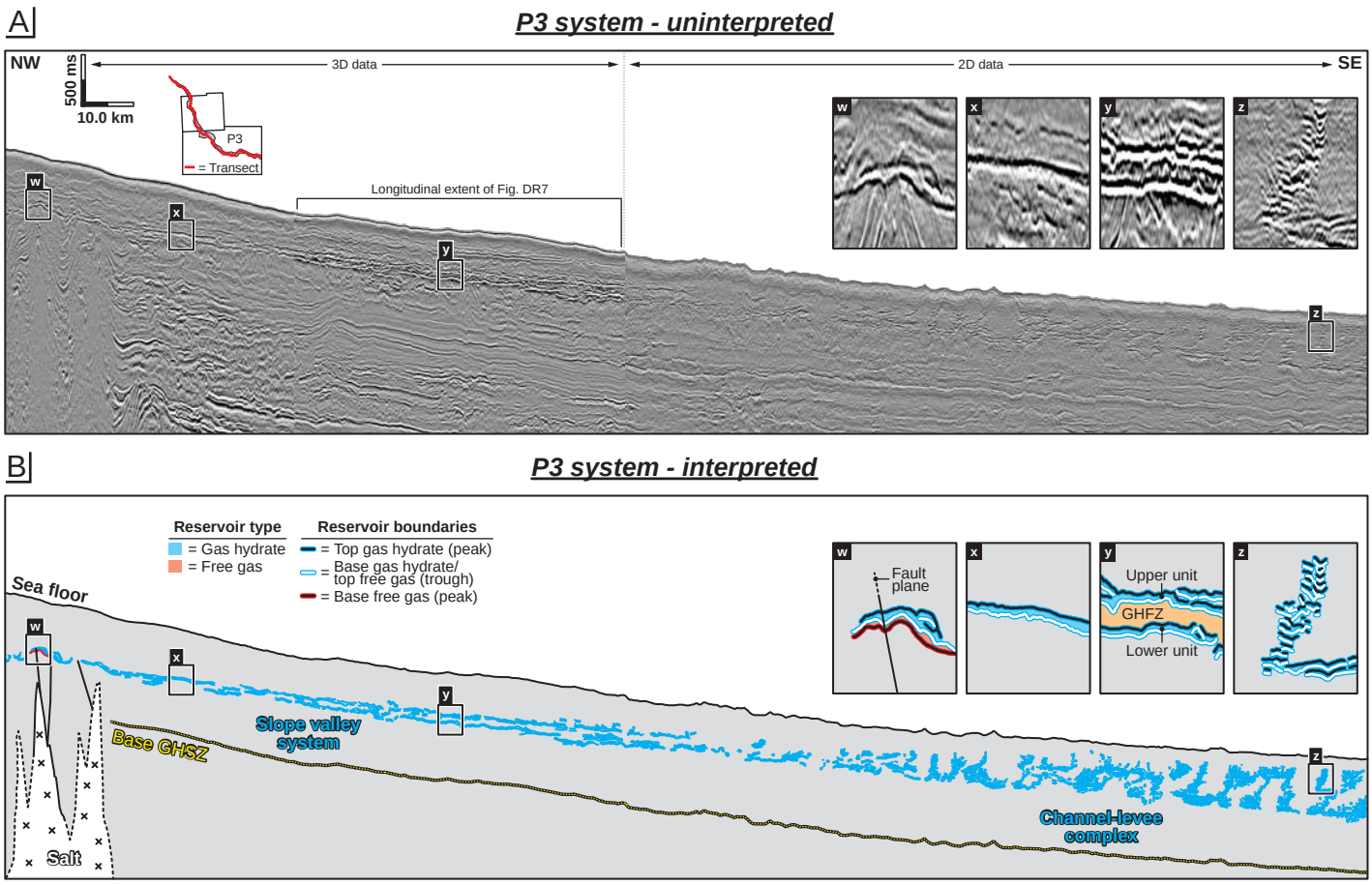

Figure DR10. Seismic traverse along the thalweg of the P3 system, showing basinward-thickening wedge-shaped reservoir. A: Uninterpreted zero-phase full-stack seismic section (TWTT). B: Interpreted section showing gas hydrate-bearing deposits of the P3 system located well above the base of the GHSZ. Towards the northwest (left), the P3 system is intersected by a fault associated with the top of a salt diapir. In medial locations, the P3 system is interpreted to consist of upper and lower reservoir units surrounding a gas hydrate free zone (GHFZ). Towards the southeast (right), the top of the P3 reservoir is situated approximately 100 ms (TWTT) below the modern sea floor.